On the small-scale fractal geometrical structure of a living coral reef barrier

Damien Sous, Frédéric Bouchette, Erik Doerflinger, Samuel Meulé, Raphael Certain, Gwladys Toulemonde, Benjamin Dubarbier, Bernard Salvat

On the small-scale fractal geometrical structure of a living coral reef barrier

Damien Sous*[1,2], Frédéric Bouchette[3,7], Erik Doerflinger[3], Samuel Meulé[4], Raphael Certain[5], Gwladys Toulemonde[6,9], Benjamin Dubarbier[7] and Bernard Salvat[8]

[1]Université de Toulon, Aix Marseille Université, CNRS, IRD, Mediterranean Institute of Oceanography (MIO), La Garde, France

[2]Univ. Pau & Pays Adour E2S UPPA, Chaire HPC Waves, Laboratoire des Sciences de l'Ingénieur Appliquées á la Mécanique et au Génie Electrique − Fédération IPRA, EA4581, Anglet, France

[3]GEOSCIENCES-M, Univ Montpellier, CNRS, Montpellier, France

[4]Aix Marseille University, CNRS, IRD, INRA, Coll France, CEREGE, Aix-en-Provence, France

[5]Université de Perpignan Via Domitia, CEFREM UMR-CNRS 5110, Perpignan, France

[6]IMAG, Univ Montpellier, CNRS, Montpellier, France

[7]GLADYS, Univ Montpellier, CNRS, Le Grau du Roi, France

[8]PSL-EPHE, CRIOBE, CNRS - UPVD - USR 3278, Université de Perpignan, France

[9]LEMON, Inria, Montpellier, France

July 7, 2020

Abstract

Topographical complexity of coral reefs is of primary importance for a number of hydrodynamical and ecological processes. The present study is based on a series of high-resolution seabottom elevation measurements along the Maupiti barrier reef, French Polynesia. Several statistical metrics and spectral analysis are used to characterize the spatial evolution of the coral geometrical structure from the reef crest to the backreef. A consistent fractal-like power law exists in the spectral density of bottom elevation for length-scales between 0.1 and 7m while, at larger scale, the reef structure shows a different pattern. Such a fine characterization of the reef geometrical structure provides key elements to reconstruct the reef history, to improve the representation of reef roughness in hydrodynamical models and to monitor the evolution of coral reef systems in the global change context.

*Corresponding author. Damien Sous, Université de Toulon, MIO/SEATECH, Bat X, Avenue de l'Université, 83130 La Garde. sous@univ-tln.fr

1 Introduction

Coral reef ecosystems are engaged on a global long-term decline trajectory. Under the combined effects of bleaching followed by partial or total destruction of the coral skeletons, sedimentation and algae covering, the structure of coral colonies will be strongly modified in the incoming years and decades (patchiness, flattening, smoothing). Research has aimed to anticipate and mitigate the degradation of coral reef systems, in particular by promoting the growth of coral on engineered structures [Clark and Edwards, 1994, Vermeij, 2006] or developing new hybrids through assisted evolution [van Oppen et al., 2015].

The related modifications of the reef biotic structure are expected to strongly affect the life cycle of many species and the physical functioning of coral reef, which shelters the inner shore from the ocean forcings. From a biological point of view, our knowledge of the geometrical structure of reef colonies is usually obtained from the identification of the involved species. Studies have related the geometry of reef colonies to their ecological functioning [Pittman and Brown, 2011, Graham and Nash, 2013, Burns et al., 2015]. The geometrical complexity is expected to being related to the health of the reef ecosystem. For instance, negative/ positive relationships have been observed between structural complexity and algal cover/ amount of living corals. Another important need is to establish a relationship between the small-scaled reef geometry and friction parameters estimated for hydrodynamical measurements (friction drag coefficient, roughness height). Such roughness parameters can be estimated from velocity and turbulence measurements [Pomeroy et al., 2017, Reidenbach et al., 2006], and are then introduced in circulation and wave numerical models [Filipot and Cheung, 2012, Hoeke et al., 2013, Pomeroy et al., 2012, Van Dongeren et al., 2013, Buckley et al., 2014, Zijlema, 2012, Buckley et al., 2014, Lashley et al., 2018, Sous et al., 2019, Yao et al., 2019]. Simple parameterizations based on geometrical features like an average height of colony have been proposed [McDonald et al., 2006, Rosman and Hench, 2011]. However, accounting for the fascinating complexity of coral reef geometry, they are, by far, not accurate enough. High-resolution morphological data in such environments are scarce and therefore our knowledge of reef geometry remains cursory. Nonetheless, a good understanding of small-scale reef geometry and relationships between such a geometry and roughness parameters would help to anticipate how degraded or man-engineered reefs may modify the habitats and the frictional properties of the shallow water reef bottom.

In additional to these functional issues, understanding and quantifiying the structural complexity of coral reefs is of primary importance in questioning the founding principles of reef formation. A series of recent studies established the statistical fractal self-similar structure of several coral reef environments from metric to kilometric scales, see e.g. [Purkis and Kohler, 2008, Schlager and Purkis, 2013, Purkis et al., 2015, Purkis et al., 2016, Duvall et al., 2019]. Synthetical terrain models based on fractional Brownian motion are able to accurately reproduce the statistical properties of complex natural reef seabeds [Purkis and Kohler, 2008]. Several development hypothesis have been formulated to explain the complexity of reef geometry. Complex reef patterns, such as reticulate "maze" reefs [Wyrwoll et al., 2006], have been first assumed to develop on antecedent high reliefs of karst topography during Pleistocene glacial sea-level lowstands [Purdy, 1974b, Purdy, 1974a]. While this antecedent karst hypothesis remains valid for some well-documented cases [Purdy et al., 2003, Purkis et al., 2010, Schlager and Purkis, 2015], it has been recently challenged by the role played by self-organisation in a number of situations [Purkis and Kohler, 2008, Schlager and Purkis, 2015]. Self-organisation is expected to be driven by biotic or combined biotic-hydrodynamical processes, allowing complex reef architecture to develop without any need for preexisting karst reliefs [Schlager and Purkis, 2015]. The driving

mechanisms and the products of spatial self-organization remains to be firmly established [Purkis et al., 2016, Purkis et al., 2015] together with consistent descriptors of the reef geometrical structure.

In this context, the aim of the present study is to provide a more comprehensive in-situ assessment of the geometrical structure of the natural and healthy coral reef barrier of a high volcanic island, which can be used as a baseline framework for understanding the reef history and the effect of ongoing and future structural modifications due to reef degradation. The approach retained here is to focus on the geometrical structure of the reef and therefore to deliberately set aside biological species-related considerations which will be involved in a future analysis to enrich and reconsider the present findings. Our analysis has been guided by a series of connected issues: Are there any dominant length-scales in the reef colony ? Can we identify universal fractal-type laws in the barrier reef geometrical structure ? What are the trends governing the spatial variability of the reef structure across a typical barrier reef ? Are there rules in the growth and nesting of a living reef over a preexisting substrate ?

For each of these issues, the documented spatial scales are determined by observations. As most studies are based on satellite or airborne measurements, the actual knowledge of reef geometry usually involves metric to kilometric scales. The higher resolution reported to date, to the authors' knowledge, was obtained by airborne Lidar topographic survey of Moorea reef barrier, French Polynesia [Duvall et al., 2019]. These observations demonstrated the multiscale and multifractal nature of the coral reef crestography. Their Lidar-based measurement spatial resolution was $1\,m$, and was designed to quantify the spectral structure of reef geometry down to length scales of $2\,m$. However, observations of natural living coral reef systems highlight structural complexity to much finer scales [Burns et al., 2015]. Focusing on a typical wave-exposed microtidal reef barrier, the objective of the present study is to conciliate two opposite ambitions : (i) describing reef geometrical structure locally as precisely as possible (at least down to the decimetric scale) and (ii) being able to provide small-scale geometrical features of the bottom over the domain extending from the reef crest to the inner lagoon. These conflicting and complex goals in terms of field operating procedures become much more complicated with the exposition of the reef to waves and currents. Such a context discards the use of aerial or submarine photogrammetry or Lidar based techniques applied in calmer and safer environments [Pittman et al., 2009, Burns et al., 2015]. Instead, a robust and more time-consuming technique has been used. The selected study site (Maupiti island reef barrier, French Polynesia) is described in section 2.1. The measurement strategy and limitations are discussed in Sec. 2.2. The results are presented in Sec. 3, while discussion and prospects are given in Sec. 4.

2 Materials and methods

2.1 Field site

The selected field site is the south-west barrier reef of the Maupiti Island. Maupiti ("the Stucked Twins") is a weakly anthropized diamond-shaped island located in the westernmost part of the Leeward Islands, Society archipelago in French Polynesia. It was selected because it can be considered as an archetypal high volcanic island, with a central island bordered by two well-developed barrier reefs on its south-east and south-west sides, two main motus (emerged vegetated areas) on the northern side that are separated by two shallow breaches (reef flat spillway or Hoa) and a single well-defined pass on its southernmost end.
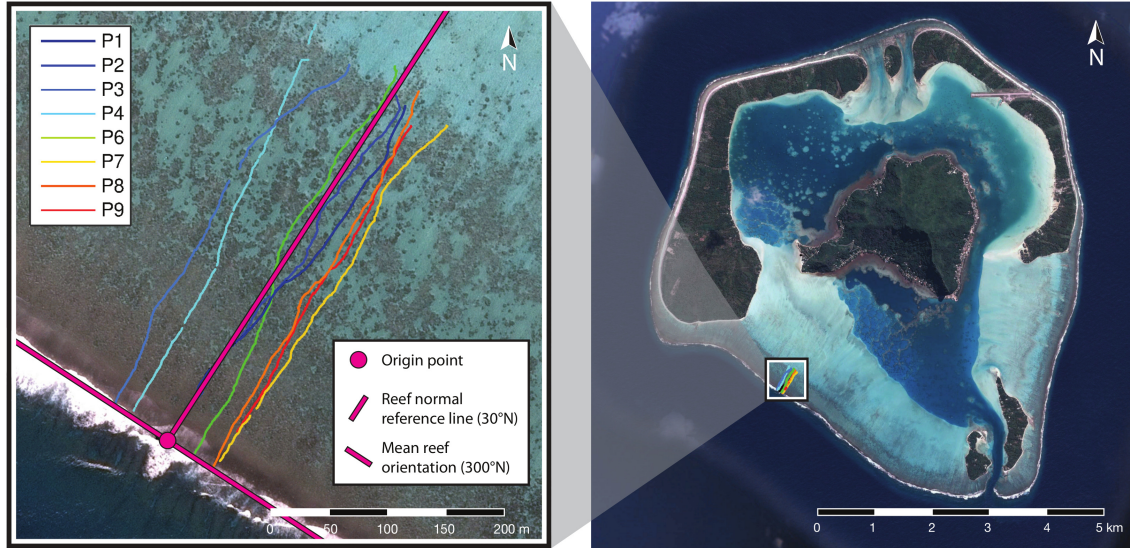
Figure 1: The Maupiti Island (right) with a zoom on the studied area showing the selected profiles (left). Image Google Earth 2018 CNES / Airbus.

The studied cross-reef zone is located in the south-west barrier. This latter area is a well-developed nearly rectilinear barrier extending over about $5\,km$ from the west motu (emerged land) to the south pass. The cross-shore structure of the selected area, which is further detailed in Section 3.1, is very representative of the reef structure observed along the 4-km long southwestern barrier reef which shows a regular alongshore structure (see Fig. 1). The acquisition area of our high-resolution topographic measurements is bounded seaside by a severe wave breaking zone which inhibited access, and at the lagoon boundary by a sharp change in topographical structure associated with the end of the well-defined coral barrier. It should be noted that the present transect does not include the reef slope, despite its interest in terms of biological activity..

2.2 Instrumentation and methods

The present analysis relies on a series of cross-shore topo-bathymetric profiles over the Maupiti barrier reef. One of the main challenges of the study was to obtain the most accurate positioning of the bed elevation in order to infer submetric statistical and spectral properties.

2.2.1 Devices and field strategy

The equipment used for altimetric surveys are GNSS (Global Navigation Satellite System) which encompasses all global position systems (GPS, GLONASS, Galileo, Beidou). In the best case, recent GNSS systems allow a positioning with a theoretical accuracy on the order of a few millimetres. In the field we used six devices, TRIMBLE R8 and R8S used two by two and deployed in Real Time Kinematics (RTK). Such a protocol is based on the coupled deployment of a base and a rover. The base is set on a fixed scaffold (a base station) and gets a reference position for all the measurements performed with the rover which is moved across the studied transect by the operator with a steel pole of known length (see Figure 2). The measurement at the
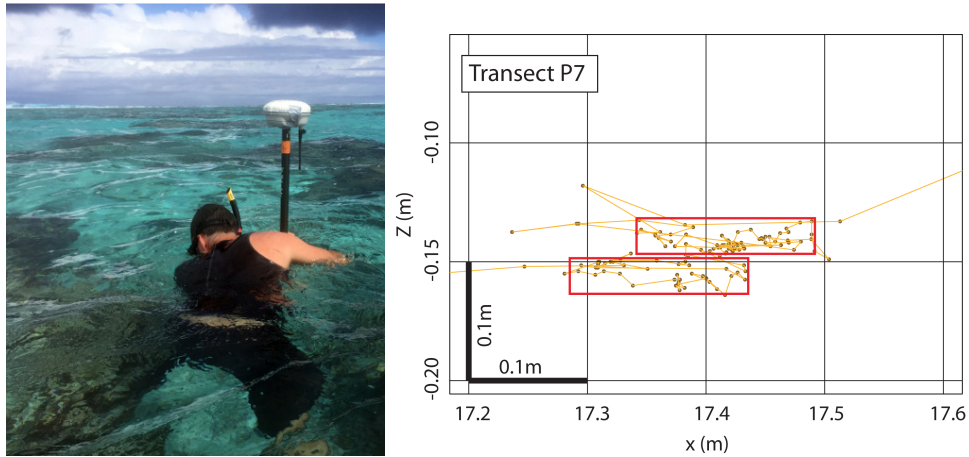
Figure 2: Left: illustration of the measurement technique. Right: raw data at two standing positions hold during the P7 profile. The red frames indicate the order of magnitude for typical measurement deviation, about 15 and 3cm for horizontal and vertical directions.

rover is corrected in real time (transmission by radio from the base) with the position measured at the base, which is assumed to be constant. If the base location is not constant, the observed difference is assumed to be reflected in both the position of the rover and the base. Thus the measurement is said differential.

The GNSS campaign relies on measurements at three distinct base stations grouped in a single network and 8 different transects numbered P1 to P9 (a P5 transect had very poor accuracy and was not used in the present analysis), located on the reef barrier, oriented approximately cross-shore and passing by the reef crest (Fig. 1). The 8 profiles are all included in a domain extending approximately $100\,m$ alongshore. In such a domain, the reef barrier is oriented $300°$ N in average. We define a reef normal reference line passing at origin point $(-16.469860°, -152.27711°)$ (WGS84) with an azimuth $30°$ N normal to the mean reef orientation (see Figure 1, a). Each transect extends from the reef crest, at the limit of safe area, to another point within the lagoon at the end of the living reef barrier, which is characterized by a depth increase and a change in topographical structure into flatter dead coral substrate covered by detritic sand and very sparse living coral elements. In order to perform the analysis and to compare between transects, transect coordinates are projected on the reference line normally with respect to the reef barrier orientation. This operation defines eight 2D cross-reef profiles representing the elevation of the seabottom with respect to the distance from a common origin at the reef crest (Fig. 3).

Different survey modes of the GNSS system have been tested. P1 and P2 were carried out with manual validation of each measurement point. P3 and P4 were performed with automatic $1\,s$ acquisition period. P6 to P9 were performed with the minimal distance/time option, i.e. a new measurement point is acquired as soon as a displacement of $0.1\,m$ is observed or a $1\,s$ time period is reached. The latter method produces much more data points than the two formers (see Tab. 1).
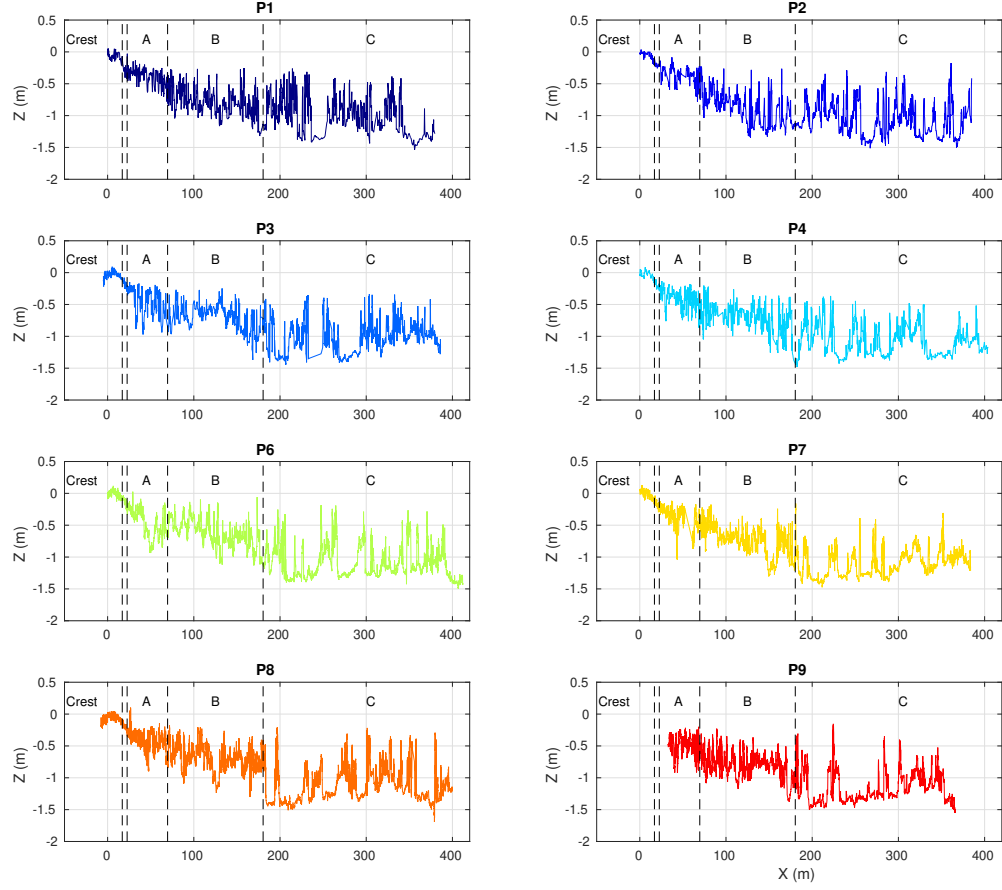
Figure 3: Measured cross-shore reef profiles.

NAME	X_{start} m	X_{end} m	GNSS mode	Nb. points	Aver. Hori. Resol. (cm)
P1	0.09	379.7	manual	1312	26
P2	0.42	385	manual	2446	16
P3	-4.99	386.2	1s automatic	2606	20
P4	0.04	403.7	1s automatic	1930	15
P6	0	412	minimal time/distance	4889	8
P7	0.35	383.8	minimal time/distance	4761	8
P8	-7.94	399.8	minimal time/distance	7102	8
P9	33	365.8	minimal time/distance	4495	9

Table 1: Profiles survey parameters

2.2.2   Spatial accuracy and resolution

The global accuracy of the topo-bathymetry surveys relies on a series of uncertainties recalled hereafter. The validity of reef geometrical analysis and recommendations for future studies are further discussed in Section 4. The instrument factory accuracy is announced at $10\,mm$ by Trimble for R8 and R8S systems. For each measurement, the survey system provides a precision for horizontal and vertical components, specifically related to the accuracy of the GNSS calculation. Considering several tens of thousands of measurements acquired in Maupiti, the RMS (Root Mean Square) and maximal offsets over the whole campaign are 10 and $25\,mm$ for horizontal components, and 29 and $59\,mm$ for vertical component. RMS and maximal offsets are provided by the GNSS software. They do comprise the uncertainly relative to the GNSS RTK metrology, but do not comprise the uncertainty relative to the operating procedure based on the moves of the operator manipulating the steel pole. An additional validation protocol has been applied in the field by repeatedly measuring the position of two control points (distinct from the base stations) on the main island. Those control points were visited six times during the campaign, i.e. before and after each field trip on the barrier. The RMS and maximal offsets calculated at those control points are 1.2 and $2.2\,cm$, 1.7 and $2\,cm$, and 1.2 and $1.9\,cm$ for north, east, and vertical components respectively. During the surveys on the reef barrier, despite all the care taken in holding the vertical of the rover's pole and continuously following the top of the canopy, the measurements are affected by the spurious motion of the operator walking along the transect. Therefore, providing a quantitative estimation of the actual uncertainty is not straightforward. A simple geometrical estimation indicates that for angles of 10° with respect to the true vertical, which in nearly the worst case observed in the field, theoretical errors can reach 35 and $5\,cm$ for horizontal and vertical components, respectively. The topographical parameters in relation with bottom elevation considered hereafter are derived from the GNSS data systematically. Thus, they embed a total uncertainty arising from all the elementary uncertainties described above. If this total uncertainty is assumed to be the sum of all the absolute values of elementary uncertainties described above, the analysis below and the calculation of all the topographical metrics deal with a worst-case principle. Following this, the total uncertainty is estimated to be $0.39\,m$ in the horizontal and $0.11\,m$ in the vertical. In practice, each source of uncertainty will not necessarily contribute its maximal possible error to the final bottom elevation accuracy. For instance the constant errors in base positioning will not affect the topographical metrics computed hereafter. Further insight is gained by a careful examination of the data during imposed standing positions held by the operator (see two examples performed on profile P7; Figure 2, right). Fluctuations are observed in the data due to the difficulty of holding a steady position measuring within the transect in the presence of severe current and/or waves. The typical order of magnitude of such spurious motions are 15 and $3\,cm$ for horizontal and vertical directions, respectively, and should be kept in mind as an overall empirical estimate of the recovered data uncertainty.

In addition to the measurement precision, the horizontal resolution is also an important parameter to discuss the validity of the geometrical laws presented later on. The resolution refers here to the density of measurement points along the surveyed transect. It is estimated by computing the averaged distance between points over the full profile. It varies between 5 and $26\,cm$ depending on the measurement configuration and the displacement speed of the operator along the profile. The spatially-averaged resolutions for each profile are given in Table 1. A spectral analysis of the measured seabottom elevations is presented in the next section. The upper boundary of the spectrum, i.e. the smaller resolved length scale, depends both on the measurement resolution and the horizontal accuracy estimated above. The robustness of the measurements is

190 further discussed in the following, but for clarity, a single lowpass frequency cutoff is applied at $10\,cm$ for all
191 presented spectra, to avoid any over-interpretation. This resolution reached by the present dataset enables
192 topographical analysis down to decimetric scales, i.e. at least ten times more accurate than Lidar-based
193 measurements [Duvall et al., 2019].

2.2.3 Data processing

195 The recovered GNSS data represent an accurate description of the seabed elevation along representative
196 cross-reef profiles. Each profile was then linearly interpolated on a regular grid ($1\,cm$ resolution). Thus, a
197 series of metric, listed below, were calculated to quantify the reef geometry.

198 - The *linear slope* was extracted from a linear fit of the bed elevation over the selected zone

199 - The *linear rugosity* was calculated as the actual distance accounting for vertical changes, i.e. the
200   sum of the individual distances between successive points, divided by the linear distance between the
201   boundaries of each selected zone [Burns et al., 2015]:

$$\frac{\sum_{i=1}^{N-1} \sqrt{(Z_{i+1} - Z_i)^2 + (X_{i+1} - X_i)^2}}{\sqrt{(Z_N - Z_1)^2 + (X_N - X_1)^2}} \tag{1}$$

202 where X and Z are the horizontal and vertical coodinates of the N selected bed points.

203 - The *standard deviation* of bottom elevation over the selected zone

$$\sqrt{\frac{1}{N-1} \sum_{i=1}^{N} (Z_i - <Z>)^2} \tag{2}$$

204 where $<.>$ is the space-averaging operator

205 - The *rate of elevational change* was computed as the averaged magnitude of elevation gradient between
206   two neighbouring points [Burns et al., 2015]

$$\frac{1}{N-1} \sum_{i=1}^{N} |\frac{Z_{i+1} - Z_i}{X_{i+1} - X_i}| \tag{3}$$

207 - The *skewness* of bottom elevation over the selected zone

$$\frac{<(Z - <Z>^3)>}{\sigma^3} \tag{4}$$

208 - The *kurtosis* of bottom elevation over the selected zone

$$\frac{<(Z - <Z>^4)>}{\sigma^4} \tag{5}$$

209 Each of the metrics were calculated for selected portions of the raw data, namely on the full profile,
210 the reef crest, and the backreef zones A, B and C described in the following section. The cross-reef spatial

Figure 4: Underwater pictures of the three zone A, B and C.

variations of mean elevation, standard deviation, skewness, and kurtosis were computed using a 500-point $(5-m)$ moving window. Computations with 100 $(1\,m)$, 200 $(2\,m)$ and 800 $(8\,m)$ points showed similar outcomes. No detrending was applied on the elevation data. For each metrics, a profile-averaged value was computed together with the standard deviation across profiles in order to assess the alongshore spatial consistency.

Further insight on the spatial structure of the reef geometry is provided by spectral analysis. A classical discrete Fast Fourier Transform was first computed, with a 10-point moving average applied on the spectral density of energy. A lowpass frequency cutoff was applied at $0.1\,m$ for each of the presented spectra. A complementary wavelet analysis was based on Haar wavelets over scales logarithmically spaced from 0.1 to $10^3\,m$. The present spectral analysis is focused on a monofractal approach in order to ensure robust comparisons with future research works [Duvall et al., 2019].

3 Results

3.1 Reef barrier zonation

The comparison of in-situ observations (Fig. 4), satellite view (Fig. 5) and measured topo-bathymetric profiles (Fig. 3) reveals the presence of several distinct areas across the reef barrier. In this section,we present a qualitative description of each zone, while more quantitative discrimination will be carried out in the following sections. The first zone, identified hereinafter as the reef crest, is the higher portion of the barrier, made of small and very compact reef colonies, containing approximately 20% of Acropora corals. The typical height of coral elements is about $20\,cm$. At the inner end of the crest, one observes a sloping transition area until the backreef is reached. This latter is divided in three successive zones which will be referred later on as zones A, B and C. Zone A extends from 22 to $70\,m$ off the reference point on the reef crest and is visually characterised by an overall slope and a compact reef structure but cracked by numerous crevasses up to $50\,cm$ deep. Acropora and Porites species represent about 20% of the coral cover. The reef compacity further decreases in zone B, extending from $70\,m$ to $180\,m$ off the reef crest, with higher, larger and more scattered reef bommies, dominated by Porites and Acropora and the presence of green algae Halimeda. This trend is accentuated when entering zone C extending from $180\,m$ to $380\,m$, where meter-high living reef pinnacles (Porites sp.) stand on a smooth dead coral bed covered by a thin layer (10-30 cm) of sand.
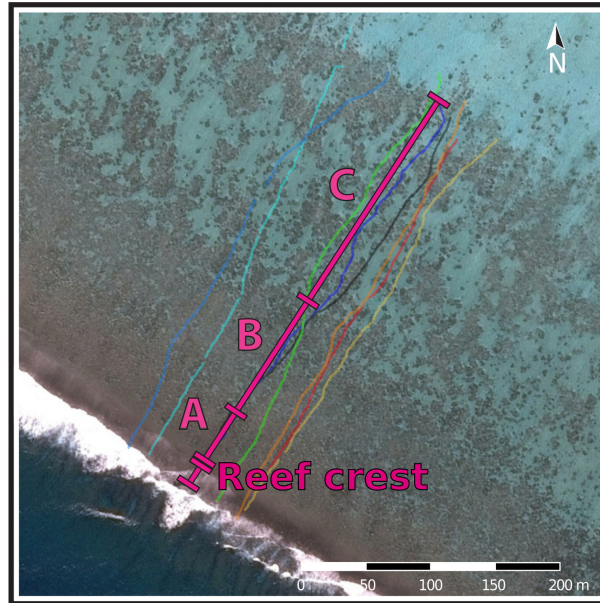
Figure 5: Satellite view of the reef zonation.

3.2 Reef geometry metrics

Table 2 presents the different metrics of bottom elevation computed on different regions of the cross-barrier profile. For each metric, the computation is performed for each profile and each zone (reef crest, full backreef and zones A, B and C) and then averaged on the profile series to provide the profile-averaged value and related standard deviation. The general trends are in general consistent across the series of profiles and well summarized by the profile-averaged values. The linear slope is observed to significantly evolve across the reef barrier. Zone C is a nearly horizontal portion of the backreef, with large coral pinnacles on a flat seabed. This contrasts with Zones A and B and reef crest which all show a negative slope (sloping toward the lagoon). The linear rugosity is quite constant all across the backreef, but shows a slightly lower value for the reef crest. The standard deviation is minimal over the reef crest and then progressively increases across the barrier. The rate of elevation change is minimal over the reef crest, reaches a maximum value in zones A and B and then slightly decreases in zone C. This latter trend is related to the fact that the rate of elevation change in zone C is generally much smaller than in other zones but affected by sparse but strong local variations. Skewness strongly varies across the barrier, with maximum and positive value for zone C and negative for all other zones while the kurtosis is much more uniform.

Summarizing, the reef crest is well discriminated from the backreef for the selected metrics of reef geometry, the only exception being the linear slope and the skewness. The discrimination of the three *a priori* identified zones from field observations is less straightforward. Linear rugosity, rate of elevational change, and kurtosis are not able to provide a quantitative discrimination of the three zones. A clearer insight is given by linear slope, standard deviation, and skewness. The basic trends are that, when moving toward the lagoon from zones A to C, the slope decreases while the standard deviation and skewness increases. The increase in standard deviation indicates an increase of the typical size of coral elements. The increase and

change in sign of skewness reveals a transition from a reef structure with narrow grooves dug into a compact reef (the so-called *d-roughness*, [Jiménez, 2004, Leonardi et al., 2007]) to a reef structure with distinct reef elements on a nearly flat bed (*k-roughness*). In zone C, the peak of elevation density is negative (about $-0.05\,m$) and the distribution is asymmetric, with more higher positive values than negative ones. In zone A, the reverse situation is observed, with a positive peak value and stronger negative tail. This indicates that the roughness structure of the backreef evolves across the profile.

Figure 6 provide further insight on the backreef spatial structure. The results are depicted for profile P9 only but are very representative of the overall trends observed. The spatial variations of bottom elevation distributions are well established, with a nearly symmetric distribution in zone B (Fig. 6, c), and negatively/positively skewed distribution for zones A/C respectively (Figs. 6, b and d). In zone A, the peak of elevation density is rather high (about $-0.5\,m$) and the distribution is asymmetric, with more high values than small ones and a heavy tail toward lower bottom elevations. In zone C, the reverse situation is observed, with a lower peak value (about $-1.3\,m$) and a pronounced tail toward higher values. This confirms the transition from *d-* to *k-roughness* reef structure when moving onshore across the reef barrier. The spatial evolution of standard deviation (Fig. 6, f), skewness (Fig. 6, g) and kurtosis (Fig. 6, h) of bottom elevation confirm the structural evolution of the reef, in particular when entering zone C where sharp fronts associated with high and well-defined pinnacles over a nearly flat bottom induce strong peaks of skewness and kurtosis.

3.3 Spectral analysis

Spectral analysis of bottom elevation was carried out to reveal the connection between the vertical and horizontal scales of reef structure. Figure 7 depicts the energy density spectra for each backreef profile. A first striking observation is the presence of a quite robust trend for each profile over a wide range, extending nearly from 0.1 to about $7\,m$ (see the straight dashed line in Figure 7). The spectral density of energy is well approximated by a power function $\alpha\Lambda^{\beta}$, where Λ is the bed wave length and α and β two data-fitted coefficients at 0.0072 and 0.92. This power law reveals the self-affine fractal-type geometrical structure of the reef barrier over a significant range of spatial scales. Near the upper boundary, for wavelengths below $0.5\,m$, a spread is observed around the mean trend and increases with decreasing wave length. This effect is likely induced by the increase of uncertainty, both related to measurement resolution and precision. No clear difference is observed between the different recording modes presented in Table 1. The observed variability may mainly be due to the local conditions of agitation and currents. For wavelengths larger than a threshold of approximately $7\,m$, the overall consistency between profiles is still satisfactory but another distinct trend is observed which does not follow the power law.

The reef zonation is demonstrated when computing the mean energy density spectra for the full backreef and the three selected zones A, B, and C depicted in black, red, blue, and green in Fig. 8, respectively. Mean spectra are obtained by averaging each spectrum. Accounting for the vertical shift due to the difference in data length, the fractal-like power law for short wavelengths is remarkably preserved for each zone. The data roll-off from the power law for the three zones occurs in the same range as for the full profile spectrum, i.e. approximately above $7\,m$. The observation of a similar roll-off threshold for different sampling lengths strengthens the idea for a true property of the seabed rather as an artifact of truncation due to an insufficient sampling length [Perline, 2005]. Significant differences between reef zones appear for larger wavelengths, the main trend being that more large scale bottom fluctuations are observed when moving away from the reef
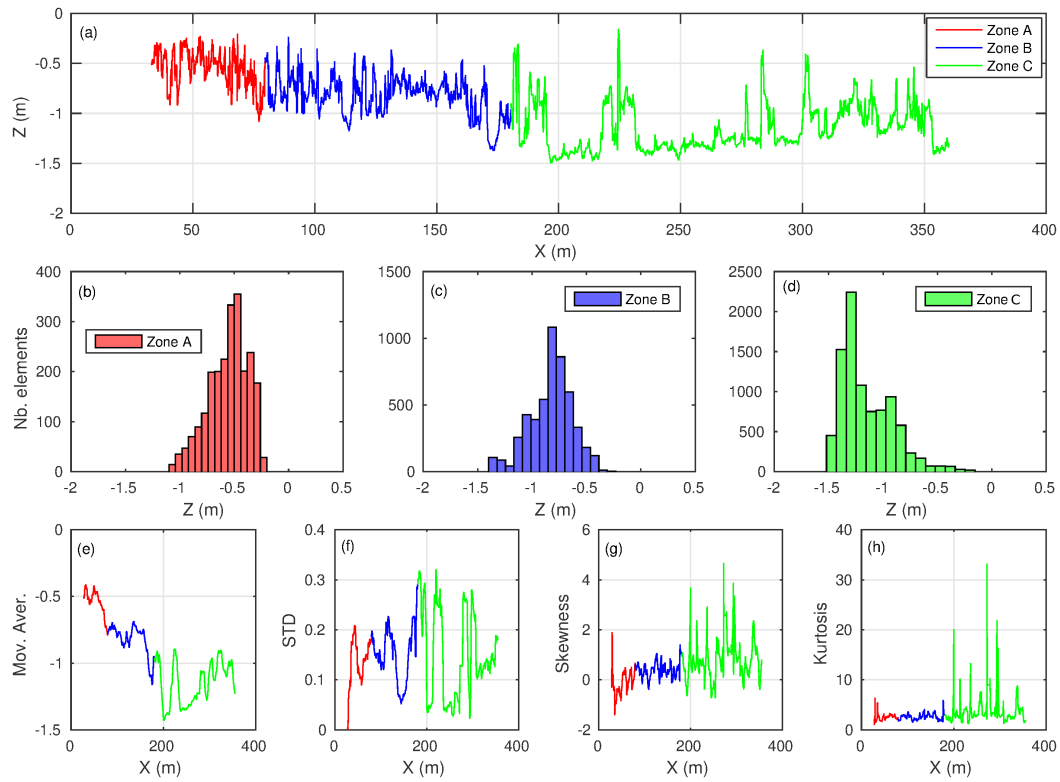
Figure 6: Reef structure metrics. (a): bottom elevation profile with the three zones A, B and C in red, blue and green, respectively. (b), (c) and (d): distribution of bottom elevations for zones A, B and C, respectively. (e), (f), (g) and (h): mean, standard deviation, skewness and kurtosis of the bottom elevation for a 500 points moving windows.
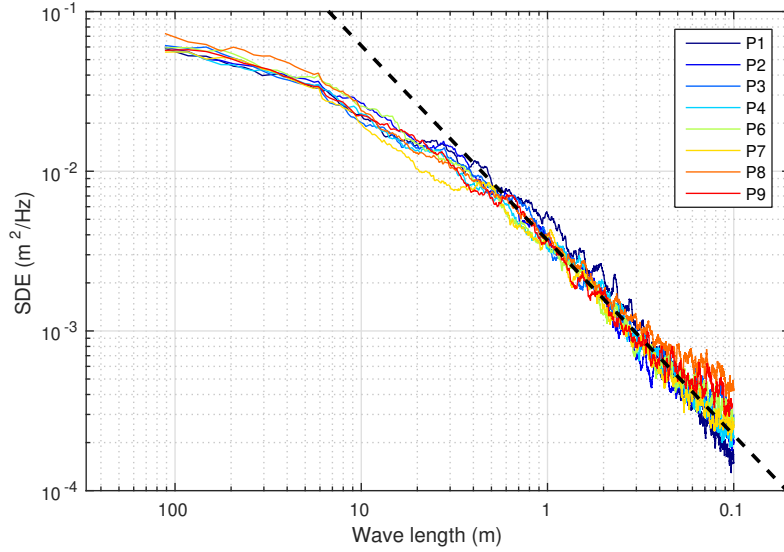
Figure 7: Energy density spectrum for bottom elevation over the full backreef for profiles P1, P2, P3, P4, P6, P7, P8 and P9.

crest. This feature is confirmed by direct visual observations in Figure 3. The reef crest data has been processed in the same manner as the backreef one. However, due to the difficulty of access to the reef crest, less measurements are available and the spectrum presented in Figure 8 is calculated only from profiles P1, P3, P6, and P8. The power law is still present for the high part of the spectrum, i.e. for wavelength range smaller than about $0.7\,m$. For larger wavelengths, the short extension of the reef crest, i.e. typically 10 to $15\,m$ wide, precludes robust interpretation.

Of particular interest is to understand the spatial connection between scales, i.e. if the coral growth tends to promote nesting and a superposition of small scales over medium or large pinnacles, or if the roughness is more evenly distributed. A wavelet distance-wavelength analysis has therefore been performed on each high resolution profile. A typical example is shown in Fig. 9 for the P8 profile. Two distinct trends can be observed. On one hand, for small wavelengths (lower than $7\,m$), a significant spatial connection is observed in the form of elongated streaks along the y-axis. On the other hand, at larger scale, the connection between scales is much less straightforward.

4 Discussion

The analysis of high resolution topo-bathymetric profiles recovered over the Maupiti island barrier reef highlights a series of original observations. Our data reveals first that the reef barrier presents a consistent self-affine geometrical fractal-like law for spatial scales lower than about $7\,m$ down to the decimetric measurement accuracy. Second, a spatial connection (colocalization) is observed for such spatial ranges while for larger wavelength spatial scales are rather disconnected. Third, the larger wavelengths are more developed when moving away from the reef crest. The present observations mark a further stage in the identification
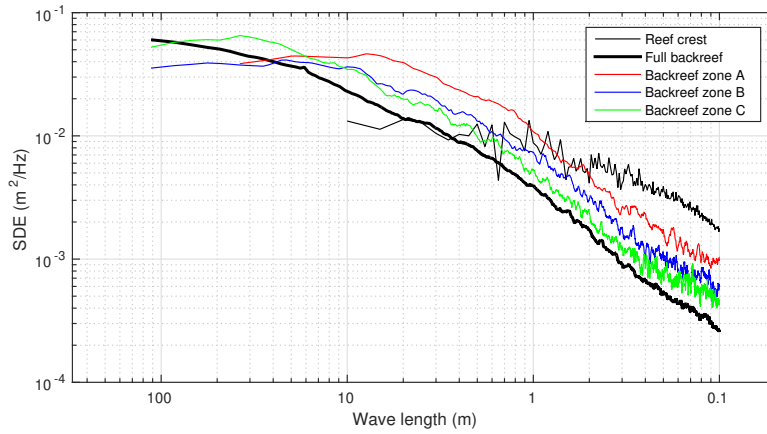
Figure 8: Energy density spectrum for backreef bottom elevation. Compiled full backreef data and selected zones A, B, and C are depicted in thick black, red, blue, and green respectively while reef crest is depicted with a thin black line.
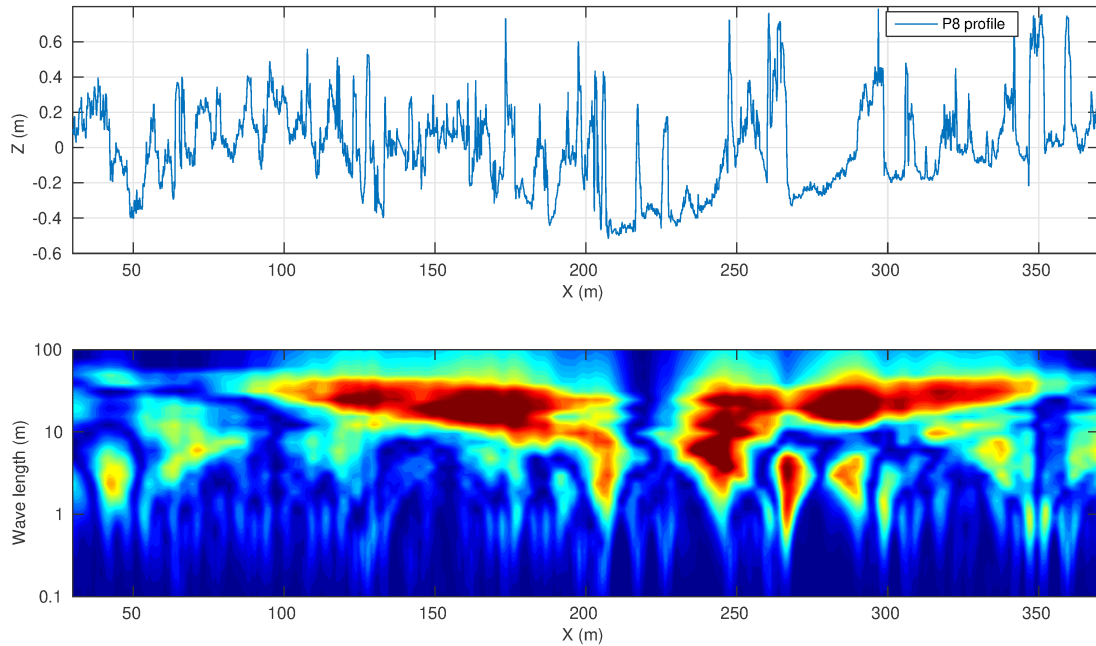

Figure 9: Top: detrended bed elevation for P8 profile. Bottom: space-frequency wavelet analysis of bed elevation across P8 profile.

of fractal-type scaling in reef contexts, reaching undocumented spatial resolution.

The identification of the driving mechanisms, from geological, biological, or hydrodynamical perspectives, for such reef structure is out of the scope of the present study, which is primarily dedicated to the geometrical structure characterization and quantification. As guidelines for further geological surveys, we proposed a hypothetical development scheme that builds on the concepts discussed at larger scale [Purkis and Kohler, 2008, Schlager and Purkis, 2015, Purkis et al., 2016]. Considering the whole Maupiti island reef-lagoon system, the current reef topography can not be univocally attributed either to antecedent Pleistocene heritage or to recent Holocene self-organization, but is likely derived from a spatially-varying combination of both mechanisms. In some locations within the lagoon, Pleistocene subaerial erosion during low water level phases is likely responsible for the formation of a complex substratum with dissolution patterns, such as incisions and pools. The growth reactivation during rewetting periods should have therefore occured on preferential locations, following the tendency for reef builders to grow preferentially on edges or topographic highs due to the turbulence-related increase of nutrient uptake [Schlager and Purkis, 2013]. This should likely explain the formation of reticulate reef systems that are observed in the southwestern and northwestern deep parts of the Maupiti lagoon. Focusing on the reef barrier studied here, the assessment of the level of connection between the present topography and the Pleistocene antecedent substratum is not straightforward from the present surveys. However, following the general insight provided by recent studies on French Polynesian wave-exposed reefs [Montaggioni et al., 2015, Gischler et al., 2019, Montaggioni et al., 2019b, Montaggioni et al., 2019a], the role of antecedent topography in the present reef structure is assumed to be weak. A series of convincing observations suggest a rather dominant effect of biotic-hydrodynamical interactions in the recent Holocene structuration.

1. The reef crest is nearly flat, made of small, healthy, and very dense colonies (Figs. 10(c,d)). Alongshore topographical surveys of the top of the reef crest, performed by classical walking DGPS procedure, showed small (10cm) and long (30-100m) undulations, but no signature of deeper antecedent substratum patterns (Fig. 10(a)).

2. The reef elements grow in size and spacing when moving from the reef crest to the backreef, leading to increasing colocalization and development of channels between interspersed but well-developed pinnacles (Fig. 10(b)). Self-organization should certainly play an important role in such cross-shore evolution. The flow channelization, which initiates just behind the reef crest and progressively increases toward the lagoon with increasing reef spacing, likely enhances the abrasion processes in the lower layers and therefore promotes the tendency of reef builders to focus growth on the highs and edges exposed to larger nutrient fluxes [Hearn et al., 2001, Schlager and Purkis, 2013, Schlager and Purkis, 2015]. The cross-shore reef structure should also directly respond to the cross-shore evolution of the hydrodynamic forcing. From the fore-reef to the reef crest, the plunging breakers induce violent hydrodynamics which acts certainly as selective constraint in the development of a compact and sturdy coralgal colony. After the reef crest, the swell energy is converted into much less intense hydrodynamics, with more regular currents and long infragravity waves which further decreases as the mean depth increases across the backreef. This allows for the growth of higher and more aerated corals, progressively across the reef.

3. Gentle reliefs, having meter to decameter horizontal length scales and decimeter to meter height scales, are conspicuous in the far backreef (zone C) and in the subsequent white sands area. These reliefs

361 often provide a base for large living coral pinnacles. It seems highly unlikely that such smoothed reliefs
362 may result from Pleistocene substratum patterns, and are more reasonably be attributed to eroded
363 bedforms developed in the detrital conglomerate consolidated during Holocene highstand periods of
364 sea-level.

365 4. The forereef (not captured in the present topographic survey but observed during calm days while
366 scuba diving) shows a peculiar structure from depths of a few meters depth up to the reef crest with
367 regular cross-shore oriented grooves about 1m wide and 1 to $3\,m$ deep (Figs. 10(f,g)), and for depths
368 beyond a few meters, the reef has a much smoother topography (Fig. 10(e)). The forereef groove
369 area is remarkably collocalized with the wave breaking zone (Fig. 10(b)). The lower forereef has a
370 regular slope with compact decimetric roughness, without any significant relief (Fig. 10(e)). Grooves
371 can be expected to focus the wave-induced currents, and act in particular as channels for the undertow
372 developing under the breaking zone [Rogers et al., 2013, Sous et al., 2020]. In their deeper part, the
373 groove walls are remarkably smooth and the groove bottoms are covered by peeble-sized debris (Fig.
374 10(g)). It can be expected that during strong wave events, the rolling debris may act as strong abrasive
375 force. The present upper forereef structure may therefore be interpreted as the signature of strong but
376 very localized interactions between reef biology and wave-induced hydrodynamics, with reef growth
377 focusing on the spurs and high flats between grooves and being inhibited within grooves by wave-
378 induced abrasion and rolling debris initially snatched from the upper living colony. The spur-groove
379 geometry on the upper part of the Maupiti forereef therefore results from a wave-driven Holocene
380 growth, as observed on Bora Bora [Gischler et al., 2019], disconnected from antecedent substratum.

381 All together, these observations suggest the idea for the combination of progradation (lateral growth)
382 and aggradation (vertical growth) both contribute to the overall Quaternary reef development, with self-
383 organizing mechanisms having a dominant role in the Holocene-active portion of the reef and a weaker role
384 of preexisting Pleistocene substratum. This is perfectly in line with the observations performed on the Bora
385 Bora windward barrier reef, akin to the Maupiti system, for which the Pleistocene substratum lies between
386 $6\,m$ and a little more than $20\,m$ below the current seabed [Gischler et al., 2019] or in the Mururoa Atoll
387 [Montaggioni et al., 2015]. In the far backreef or further into the lagoon (white sand area), the Pleistocene
388 substratum may be closer to the present seabed and may also play a role in the living reef geometrical
389 structure. Additional seismic imagery and geochronological surveys are planned to provide more insight
390 on the spatial history of the barrier reef development and inform on how antecedent substratum and self-
391 organization contribute to the present reef topographical structure.

392 The present methodology gave access to decimetric length scales, therefore extending the recent analysis
393 of the Moorea reef presented by Duvall et al. [Duvall et al., 2019]. Our results confirm and extend, at small
394 scale, the Moorea reef observations [Duvall et al., 2019] that topographical structure shows strong spatial
395 variations which can not be captured by part of the common metrics. In the length scale range 0.1 to $7\,m$,
396 monofractal analysis are very robust and are expected to provide a reference database to test the existence
397 of such a law in other coral reef sites and to discuss its dependency on the reef context, in terms of history,
398 forcing, and biology. The extension of the measurement range down to the smallest (millimeter) scales of the
399 reef colony is a challenging task. Considering the care taken in the present series of surveys, it seems that the
400 measurement accuracy can hardly be further improved with similar techniques. Other strategies may be con-
401 sidered, such as photogrammetry or High Resolution laser scanning [Pittman et al., 2009, Burns et al., 2015],

402 and adapted to the particular contexts of fringing and barrier reefs. The future survey area should extend
403 onto both the forereef and inner lagoon to provide similar characterization of those areas. The forereef slope is
404 of primary importance because it is the crucible of intense interactions between biology and hydrodynamics.
405 However, the forereef remains a major metrological challenge due to the harshness of the environment and
406 strong wave exposure. The alongshore reef structure also deserves dedicated exploration to confirm that the
407 profiles selected here are representative of the whole barrier system. Additionally longer topographic surveys
408 will provide higher resolution of the longer wavelengths and minimize truncation effects [Perline, 2005].

409 The presence of a spectral deviation for length scales of approximately $7\,m$ is attributed to the su-
410 perposition of a living coral colony over a smoothly undulating substratum. The spectral deviation calls
411 for a series of remarks concerning the implications for hydrodynamical processes. Until now, most of
412 the modeling studies dedicated to reef barrier or fringing reefs have assumed a spatially uniform friction
413 coefficient [Filipot and Cheung, 2012, Hoeke et al., 2013, Pomeroy et al., 2012, Van Dongeren et al., 2013,
414 Buckley et al., 2014, Zijlema, 2012, Buckley et al., 2014, Sous et al., 2019, Sous et al., 2020]. While such an
415 approach provides a decent representation of wave transformation and momentum balance after a proper cal-
416 ibration, this remains unsatisfactory in the light of the present observation of a strong cross-shore evolution of
417 the reef geometrical structure in the vertical and horizontal length scales of the roughness, and even the rough-
418 ness type. Both vertical and horizontal length scales tend to increase when moving away from the reef crest
419 while the roughness type evolves from a d-type to a k-type roughness. This should play an important role in
420 the flow dynamics, particularly in terms of stability and relative contributions of frictional drag and pressure
421 drag [Jiménez, 2004]. The implementation of spatially-distributed reef roughness appears therefore a neces-
422 sary step, particularly when considering the present research effort to increase the accuracy of wave models in
423 coral reef environments, see e.g. [Lashley et al., 2018, Sous et al., 2019, Sous et al., 2020, Yao et al., 2020].
424 Direct local measurements of bottom friction can significantly differ from the bulk friction coefficient ob-
425 tained from model calibration, emphasising the need to account for spatial variations of the reef structure
426 and the resulting modifications of frictional processes. In addition, this latter connection between reef struc-
427 ture and friction parameters remains a challenging issue. Most of the current approaches relies on a single
428 bottom drag coefficient, either constant or depth-dependent [McDonald et al., 2006, Sous et al., 2020], with
429 a significant spread of values both measured in the field or used in the models [Rosman and Hench, 2011].
430 Roughness is generally described either by a "discrete" approach, i.e. by a combination of roughness ele-
431 ment scales such as height, width, and spacing, or by a "continuous" approach through statistical moments
432 and moment functions [Stewart et al., 2019]. While the former approach should be restricted to simple reg-
433 ular roughness, more complex surface roughness are often treated similarly by assuming the existence of
434 an equivalent roughness height [Schlichting and Gersten, 2016]. Due to the complexity of coral reef, more
435 robust "continuous" approaches, which have been shown to provide finer descriptor of complex surfaces
436 [Flack and Schultz, 2010], should be considered. It is only very recently that the effect of the spectral struc-
437 ture of bed elevation on the hydraulic resistance has been explored by dedicated small-scale laboratory
438 experiments on synthetic self-affine surfaces [Stewart et al., 2019]. These observations highlight the impor-
439 tance of the spectral power law, which leads to an increase of friction for a decreasing spectral exponent.
440 Further developments and extensive comparisons with hydrodynamic measurements are therefore required
441 to integrate the complexity of the reef crestographic structure described here into hydrodynamic parameters.
442 In addition, the parameterization of friction in numerical models should be considered in view of the de-

sired model resolution and the available bathymetric data. Based on the present observations, models with multi-decametric resolution must parameterize the friction associated with the decametric reef crestographic features while models with metric resolution can explicitly represent them and only parameterize submetric features. Considering the spectral structure of the reef geometry, an interesting approach may be to capture the large wavelengths of the seafloor associated with the dead reef substratum both through bathymetric surveys, which remain accessible to common echosounder measurements, and adequate numerical model resolution while, at smaller scales, to properly parameterize the hydrodynamic effect of the living reef roughness, accounting for the spatial variability and the fractal geometry. This latter prospect is outside the scope of the present study, but will be further explored in the processing of hydrodynamical data recovered on the Maupiti reef barrier during the Maupiti Hoé 2018 experiment. It should also be noted that the reef structural complexity here isonly addressed in terms of surface elevation. Although the present approach is already a metrological challenge, it does not account for the inner structure of the coral colony. The degree of connectedness within the coral colony, related to physical properties such as porosity, tortuosity, or specific surface [Arnaud et al., 2017], will necessarily affect the flow structure and the related head loss, particularly for shallow environments [Monismith, 2014, Rosman and Hench, 2011]. While the fine 3D envelope of the coral colony should certainly be measured by dedicated photogrammetry or laser strategies [Pittman et al., 2009, Burns et al., 2015], the estimation of the inner porous properties for a real coral reef at the field scale remains, to the author's knowledge, out of reach for conventional technologies.

Finally, an additional prospect of considerable ecological importance will be to survey the evolution of the reef geometrical structure under the global reef degradation process. Reduction of reef structural complexity and algae covering will both impact the wave and current attenuation provided by reefs, with strong expected consequences on erosion and submersion events, and the health of the reef-lagoon ecosystem.

5 Conclusion

Characterizing the complexity of coral reef crestography is of primary importance in the context of global reef degradation, including the understanding of the role of reefs in shore protection and the preservation of the health of reef-lagoon ecosystems.

A series of high resolution cross-barrier topographic surveys have been carried out on the Maupiti reef barrier, French Polynesia. The measurement strategy allowed for decimetric resolution. The observations confirmed and extended to smaller scales the analysis performed by Duvall et al. [Duvall et al., 2019] on the Moorea reef. The reef geometry shows strong spatial variations across the barrier, which are only partly represented by common roughness metrics. The distribution of reef bottom elevations reveals a transition from d-type to a k-type roughness across the reef barrier. The spectral analysis highlights the presence of a robust monofractal power law in the range 0.1 to $7\,m$. A different pattern is observed at larger length scale, suggesting that the reef geometrical structure relies on the superposition of alive corals over the reliefs of a consolidated detrital substratum. The present barrier reef topography appears to be mainly controlled by Holocene self-organizing growth rather than by the Pleistocene geological heritage. Further investigations will be carried out to connect the present observations with the hydrodynamical properties and to provide a general framework for numerical modeling of reef-lagoon systems.
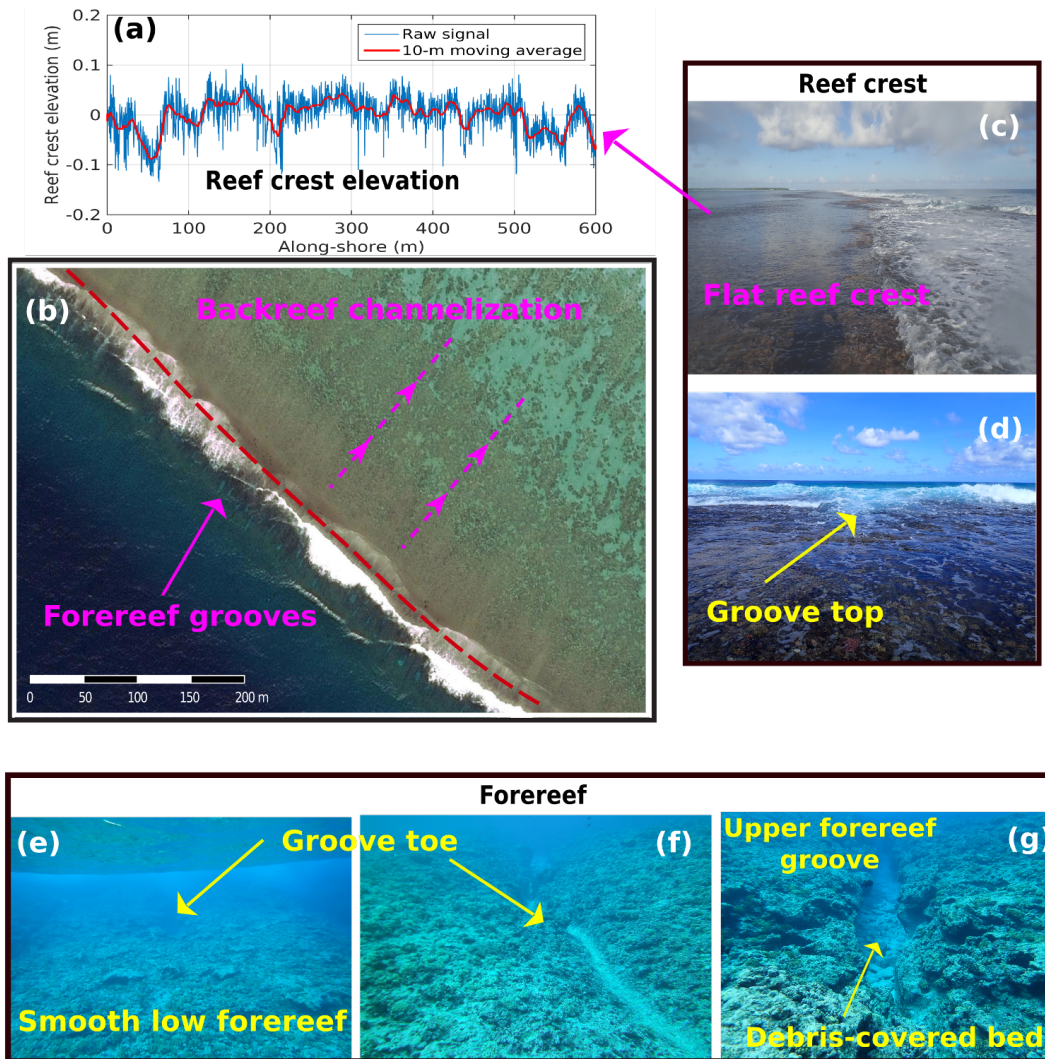
Figure 10: Holocene-grown barrier reef structure. (a): Reef crest elevation from topographic survey along the red line in (b), raw and smoothed data are in blue and red lines, respectively. (b): Barrier reef satellite view with visible spur-groove structure of the upper forereef and current-induced chenalization initiating behind the reef crest. (c): Reef crest picture (south-eastward). (d): Reef crest picture showing the top of a forereef groove, note that the groove does not notch the crest. (e): Lower forereef. (f): Forereef picture showing a typical groove toe. (g): Forereef groove partially filled with peeble-sized debris.

Acknowledgments

Data availability statement

The data sets used and/or analyzed during the current study are available from the corresponding author on reasonable request.

Declaration of Conflicting Interest

The Authors declare that there is no conflict of interest

Metrics	Zone	Profile-averaged	Profile STD	P1	P2	P3	P4	P6	P7	P8	P9
Linear Slope (.10^{-3})	Crest	-4.5	2.8	-2	-7.7	-3.5	-4.7	-4.2	-8.4	-5.7	-
	A	-6	1.1	-7	-7	-7.4	-4.8	-4.5	-5.8	-5.2	-6.2
	B	-3.3	0.093	-3.1	-4.1	-3	-3.8	-4.2	-3.8	-1.4	-2.7
	C	-0.23	1.3	-1.4	-1.2	-1	-0.8	0.1	1.3	2.2	0.7
	Full	-2.5	0.25	-2.5	-2.6	-2.4	-2.8	-2.8	-2.7	-2.4	-2.1
Linear Rugosity	Crest	1.051	0.041	1.0299	1.011	1.0213	1.0115	1.0867	1.102	1.094	-
	A	1.243	0.146	1.126	1.094	1.16	1.267	1.141	1.239	1.413	1.5
	B	1.254	0.139	1.18	1.156	1.245	1.175	1.222	1.273	1.547	1.354
	C	1.218	0.095	1.216	1.169	1.2619	1.126	1.247	1.131	1.416	1.174
	Full	1.222	0.0938	1.18	1.143	1.193	1.155	1.213	1.186	1.432	1.276
Standard Deviation	Crest	0.05	0.0058	0.355	0.051	0.042	0.05	0.051	0.057	0.0439	-
	A	0.185	0.019	0.172	0.179	0.221	0.171	0.209	0.179	0.166	0.182
	B	0.199	0.016	0.193	0.221	0.18	0.209	0.211	0.208	0.176	0.195
	C	0.244	0.0225	0.274	0.245	0.24	0.242	0.252	0.199	0.267	0.236
	Full	0.363	0.024	0.356	0.372	0.356	0.371	0.387	0.378	0.378	0.309
Rate Elev. Change	Crest	0.217	0.113	0.147	0.108	0.161	0.097	0.321	0.337	0.347	-
	A	0.517	0.199	0.367	0.286	0.408	0.55	0.391	0.526	0.747	0.862
	B	0.52	0.186	0.412	0.374	0.332	0.412	0.494	0.552	0.893	0.66
	C	0.429	0.116	0.117	0.377	0.477	0.309	0.475	0.321	0.67	0.37
	Full	0.455	0.123	0.397	0.345	0.407	0.363	0.457	0.419	0.724	0.532
Skewness	Crest	-0.241	0.361	-0.1799	-0.945	0.083	-0.461	-0.113	0.0857	-0.158	-
	A	-0.634	0.399	-1.289	-0.985	-0.167	-0.852	-0.323	-0.709	-0.207	-0.537
	B	-0.379	0.392	-0.137	0.151	-0.62	-1.091	-0.016	-0.565	-0.336	-0.425
	C	0.71	0.272	0.308	0.534	0.496	0.564	1.025	0.918	0.783	1.043
	Full	0.33	0.127	0.258	0.545	0.311	0.275	0.3	0.511	0.204	0.235
Kurtosis	Crest	2.67	0.395	2.582	3.273	2.632	3.137	2.177	2.442	2.447	-
	A	3	0.84	4.521	3.349	1.791	3.423	2.11	3.088	2.986	2.74
	B	3.051	0.534	2.945	2.227	3.029	4.089	2.718	2.881	3.255	3.261
	C	2.919	0.671	2.209	2.531	2.481	2.264	3.192	3.89	2.936	3.843
	Full	2.278	1.151	2.379	2.395	2.485	2.269	2.105	2.334	2.215	2.047

Table 2: Metrics of reef geometry for the reef crest and the backreef (Zones A, B, C and full backreef). Results are given for each profile P1 to P9 and averaged over the profiles.

References

[Arnaud et al., 2017] Arnaud, G., Rey, V., Touboul, J., Sous, D., Molin, B., and Gouaud, F. (2017). Wave propagation through dense vertical cylinder arrays: Interference process and specific surface effects on damping. *Applied Ocean Research*, 65:229–237.

[Buckley et al., 2014] Buckley, M., Lowe, R., and Hansen, J. (2014). Evaluation of nearshore wave models in steep reef environments. *Ocean Dynamics*, 64(6):847–862.

[Burns et al., 2015] Burns, J., Delparte, D., Gates, R., and Takabayashi, M. (2015). Integrating structure-from-motion photogrammetry with geospatial software as a novel technique for quantifying 3d ecological characteristics of coral reefs. *PeerJ*, 3:e1077.

[Clark and Edwards, 1994] Clark, S. and Edwards, A. J. (1994). Use of artificial reef structures to rehabilitate reef flats degraded by coral mining in the maldives. *Bulletin of Marine Science*, 55(2-3):724–744.

[Duvall et al., 2019] Duvall, M. S., Hench, J. L., and Rosman, J. H. (2019). Collapsing complexity: quantifying multi-scale properties of reef topography. *Journal of Geophysical Research: Oceans*, 124:5021–5038.

[Filipot and Cheung, 2012] Filipot, J.-F. and Cheung, K. F. (2012). Spectral wave modeling in fringing reef environments. *Coastal Engineering*, 67:67–79.

[Flack and Schultz, 2010] Flack, K. A. and Schultz, M. P. (2010). Review of hydraulic roughness scales in the fully rough regime. *Journal of Fluids Engineering*, 132(4).

[Gischler et al., 2019] Gischler, E., Hudson, J. H., Humblet, M., Braga, J. C., Schmitt, D., Isaack, A., Eisenhauer, A., and Camoin, G. F. (2019). Holocene and pleistocene fringing reef growth and the role of accommodation space and exposure to waves and currents (bora bora, society islands, french polynesia). *Sedimentology*, 66(1):305–328.

[Graham and Nash, 2013] Graham, N. and Nash, K. (2013). The importance of structural complexity in coral reef ecosystems. *Coral Reefs*, 32(2):315–326.

[Hearn et al., 2001] Hearn, C., Atkinson, M., and Falter, J. (2001). A physical derivation of nutrient-uptake rates in coral reefs: effects of roughness and waves. *Coral Reefs*, 20(4):347–356.

[Hoeke et al., 2013] Hoeke, R. K., Storlazzi, C. D., and Ridd, P. V. (2013). Drivers of circulation in a fringing coral reef embayment: a wave-flow coupled numerical modeling study of hanalei bay, hawaii. *Continental Shelf Research*, 58:79–95.

[Jiménez, 2004] Jiménez, J. (2004). Turbulent flows over rough walls. *Annu. Rev. Fluid Mech.*, 36:173–196.

[Lashley et al., 2018] Lashley, C. H., Roelvink, D., van Dongeren, A., Buckley, M. L., and Lowe, R. J. (2018). Nonhydrostatic and surfbeat model predictions of extreme wave run-up in fringing reef environments. *Coastal Engineering*, 137:11–27.

[Leonardi et al., 2007] Leonardi, S., Orlandi, P., and Antonia, R. A. (2007). Properties of d-and k-type roughness in a turbulent channel flow. *Physics of fluids*, 19(12):125101.

[McDonald et al., 2006] McDonald, C., Koseff, J., and Monismith, S. (2006). Effects of the depth to coral height ratio on drag coefficients for unidirectional flow over coral. *Limnology and oceanography*, 51(3):1294–1301.

[Monismith, 2014] Monismith, S. G. (2014). Flow through a rough, shallow reef. *Coral Reefs*, 33(1):99–104.

[Montaggioni et al., 2015] Montaggioni, L. F., Borgomano, J., Fournier, F., and Granjeon, D. (2015). Quaternary atoll development: New insights from the two-dimensional stratigraphic forward modelling of mururoa island (central pacific ocean). *Sedimentology*, 62(2):466–500.

[Montaggioni et al., 2019a] Montaggioni, L. F., Collin, A., James, D., Salvat, B., Martin-Garin, B., Siu, G., Taiarui, M., and Chancerelle, Y. (2019a). Morphology of fore-reef slopes and terraces, takapoto atoll (tuamotu archipelago, french polynesia, central pacific): The tectonic, sea-level and coral-growth control. *Marine Geology*, 417:106027.

[Montaggioni et al., 2019b] Montaggioni, L. F., Salvat, B., Aubanel, A., Pons-Branchu, E., Martin-Garin, B., Dapoigny, A., and Goeldner-Gianella, L. (2019b). New insights into the holocene development history of a pacific, low-lying coral reef island: Takapoto atoll, french polynesia. *Quaternary Science Reviews*, 223:105947.

[Perline, 2005] Perline, R. (2005). Strong, weak and false inverse power laws. *Statistical Science*, pages 68–88.

[Pittman and Brown, 2011] Pittman, S. J. and Brown, K. A. (2011). Multi-scale approach for predicting fish species distributions across coral reef seascapes. *PloS one*, 6(5):e20583.

[Pittman et al., 2009] Pittman, S. J., Costa, B. M., and Battista, T. A. (2009). Using lidar bathymetry and boosted regression trees to predict the diversity and abundance of fish and corals. *Journal of Coastal Research*, pages 27–38.

[Pomeroy et al., 2012] Pomeroy, A., Lowe, R., Symonds, G., Van Dongeren, A., and Moore, C. (2012). The dynamics of infragravity wave transformation over a fringing reef. *Journal of Geophysical Research: Oceans (1978–2012)*, 117(C11).

[Pomeroy et al., 2017] Pomeroy, A. W., Lowe, R. J., Ghisalberti, M., Storlazzi, C., Symonds, G., and Roelvink, D. (2017). Sediment transport in the presence of large reef bottom roughness. *Journal of Geophysical Research: Oceans*, 122(2):1347–1368.

[Purdy, 1974a] Purdy, E. G. (1974a). Karst-determined facies patterns in british honduras: Holocene carbonate sedimentation model. *AAPG Bulletin*, 58(5):825–855.

[Purdy, 1974b] Purdy, E. G. (1974b). Reef configurations: cause and effect.

[Purdy et al., 2003] Purdy, E. G., Gischler, E., and Lomando, A. J. (2003). The belize margin revisited. 2. origin of holocene antecedent topography. *International Journal of Earth Sciences*, 92(4):552–572.

[Purkis et al., 2015] Purkis, S., Casini, G., Hunt, D., and Colpaert, A. (2015). Morphometric patterns in modern carbonate platforms can be applied to the ancient rock record: Similarities between modern alacranes reef and upper palaeozoic platforms of the barents sea. *Sedimentary Geology*, 321:49–69.

[Purkis and Kohler, 2008] Purkis, S. J. and Kohler, K. E. (2008). The role of topography in promoting fractal patchiness in a carbonate shelf landscape. *Coral Reefs*, 27(4):977.

[Purkis et al., 2016] Purkis, S. J., Koppel, J. V. D., and Burgess, P. M. (2016). Spatial Self-Organization in Carbonate Depositional Environments. In *Autogenic Dynamics and Self-Organization in Sedimentary Systems*. SEPM Society for Sedimentary Geology.

[Purkis et al., 2010] Purkis, S. J., Rowlands, G., Riegl, B., and Renaud, P. (2010). The paradox of tropical karst morphology in the coral reefs of the arid middle east. *Geology*, 38(3):227–230.

[Reidenbach et al., 2006] Reidenbach, M. A., Monismith, S. G., Koseff, J. R., Yahel, G., and Genin, A. (2006). Boundary layer turbulence and flow structure over a fringing coral reef. *Limnology and Oceanography*, 51(5):1956.

[Rogers et al., 2013] Rogers, J. S., Monismith, S. G., Feddersen, F., and Storlazzi, C. D. (2013). Hydrodynamics of spur and groove formations on a coral reef. *Journal of Geophysical Research: Oceans*, 118(6):3059–3073.

[Rosman and Hench, 2011] Rosman, J. H. and Hench, J. L. (2011). A framework for understanding drag parameterizations for coral reefs. *Journal of Geophysical Research: Oceans*, 116(C8).

[Schlager and Purkis, 2015] Schlager, W. and Purkis, S. (2015). Reticulate reef patterns–antecedent karst versus self-organization. *Sedimentology*, 62(2):501–515.

[Schlager and Purkis, 2013] Schlager, W. and Purkis, S. J. (2013). Bucket structure in carbonate accumulations of the maldive, chagos and laccadive archipelagos. *International Journal of Earth Sciences*, 102(8):2225–2238.

[Schlichting and Gersten, 2016] Schlichting, H. and Gersten, K. (2016). *Boundary-layer theory*. Springer.

[Sous et al., 2020] Sous, D., Dodet, G., Bouchette, F., and Tissier, M. (2020). Momentum balance over a barrier reef. *Journal of Geophysical Research: Oceans*, DOI: 10.1029/2019JC015503.

[Sous et al., 2019] Sous, D., Tissier, M., Rey, V., Touboul, J., Bouchette, F., Devenon, J.-L., Chevalier, C., and Aucan, J. (2019). Wave transformation over a barrier reef. *Continental Shelf Research*, 184:66–80.

[Stewart et al., 2019] Stewart, M. T., Cameron, S. M., Nikora, V. I., Zampiron, A., and Marusic, I. (2019). Hydraulic resistance in open-channel flows over self-affine rough beds. *Journal of Hydraulic Research*, 57(2):183–196.

[Van Dongeren et al., 2013] Van Dongeren, A., Lowe, R., Pomeroy, A., Trang, D. M., Roelvink, D., Symonds, G., and Ranasinghe, R. (2013). Numerical modeling of low-frequency wave dynamics over a fringing coral reef. *Coastal Engineering*, 73:178–190.

[van Oppen et al., 2015] van Oppen, M. J., Oliver, J. K., Putnam, H. M., and Gates, R. D. (2015). Building coral reef resilience through assisted evolution. *Proceedings of the National Academy of Sciences*, 112(8):2307–2313.

[Vermeij, 2006] Vermeij, M. (2006). Early life-history dynamics of caribbean coral species on artificial substratum: the importance of competition, growth and variation in life-history strategy. *Coral Reefs*, 25(1):59–71.

[Wyrwoll et al., 2006] Wyrwoll, K.-H., Zhu, Z. R., Collins, L. B., and Hatcher, B. G. (2006). Origin of blue hole structures in coral reefs: Houtman abrolhos, western australia. *Journal of Coastal Research*, pages 202–208.

[Yao et al., 2020] Yao, Y., Zhang, Q., Becker, J. M., and Merrifield, M. A. (2020). Boussinesq modeling of wave processes in field fringing reef environments. *Applied Ocean Research*, 95:102025.

[Yao et al., 2019] Yao, Y., Zhang, Q., Chen, S., and Tang, Z. (2019). Effects of reef morphology variations on wave processes over fringing reefs. *Applied Ocean Research*, 82:52–62.

[Zijlema, 2012] Zijlema, M. (2012). Modelling wave transformation across a fringing reef using swash. *Coastal Engineering Proceedings*, 1(33):26.